Electronic Supplementary Material (ESI) for Journal of Materials Chemistry A.

Self-adhesive Polyzwitterionic Hydrogel Electrolytes for Long-life Flexible Zinc-ion Batteries

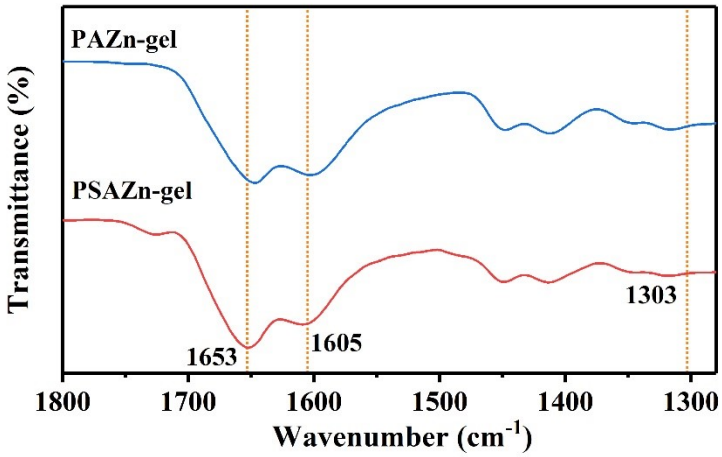

Figure S1. Localized view of FTIR spectra of PSAZn-gel and PAZn-gel.

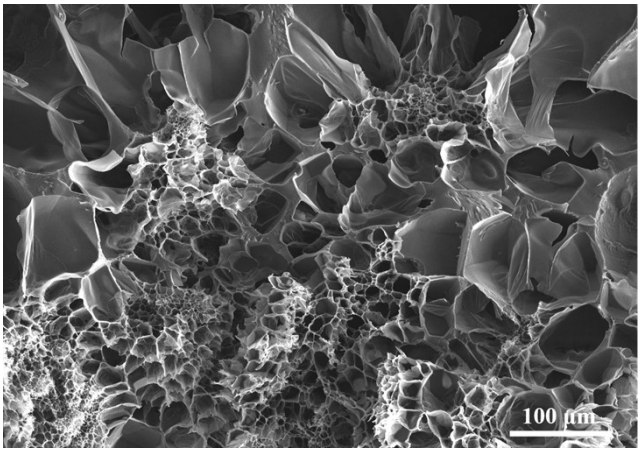

Figure S2. Cross-section SEM image of PAZn-gel.

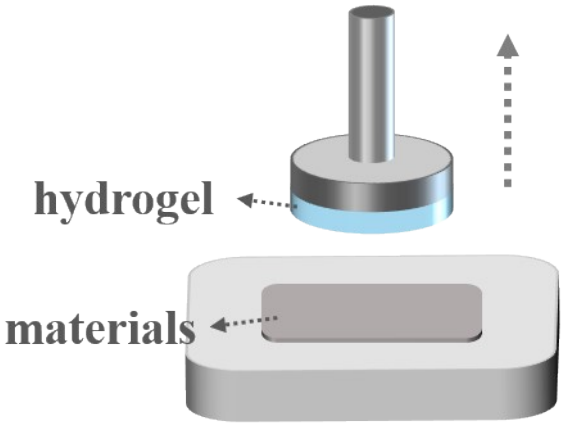

Figure S3. Schematic diagram of adhesion strength test method

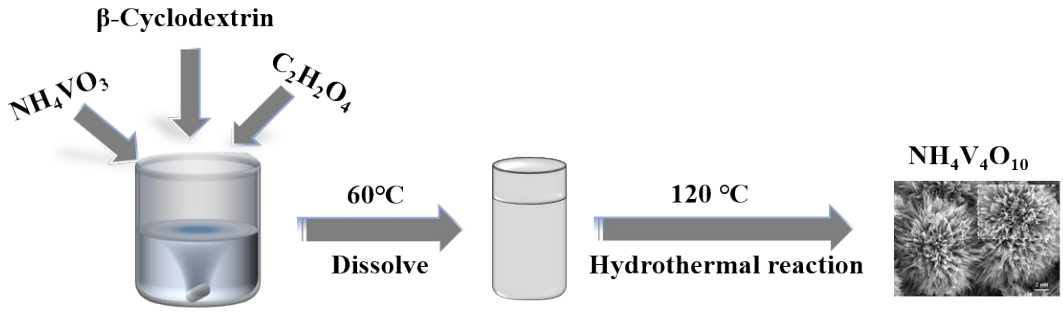

Figure S4. process flow diagram for the preparation of NHVO

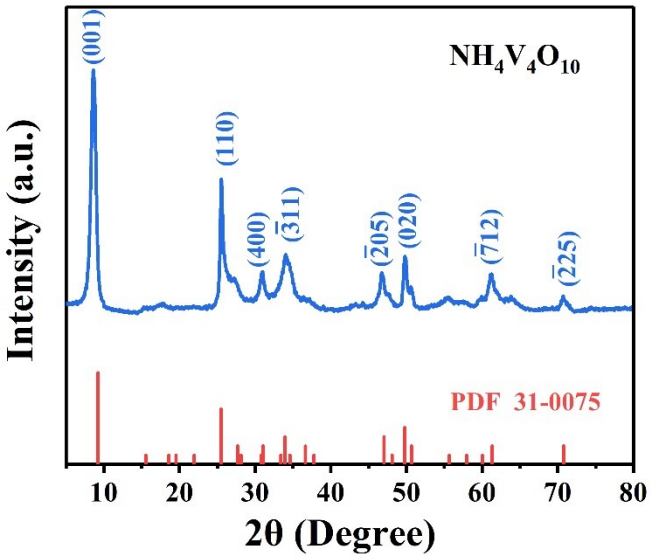

Figure S5. XRD pattern of NHVO

The structure of the synthesized material was determined by X-ray diffraction (XRD) analysis, and the structure of the obtained material was determined to be $NH_4V_4O_{10}$ by comparison with the standard PDF card (PDF 31-0075)

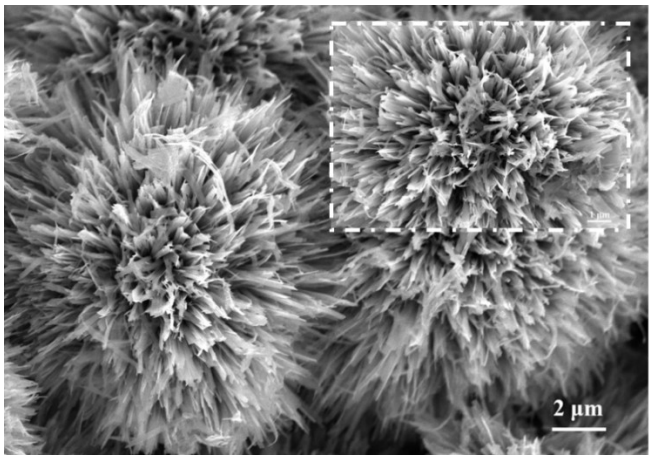

Figure S6. SEM image of the NHVO

The SEM image clearly shows that the synthesized ammonium vanadate exhibits a uniform nanoflower-like structure, which has a large specific surface area and helps to increase the specific capacity of the battery.

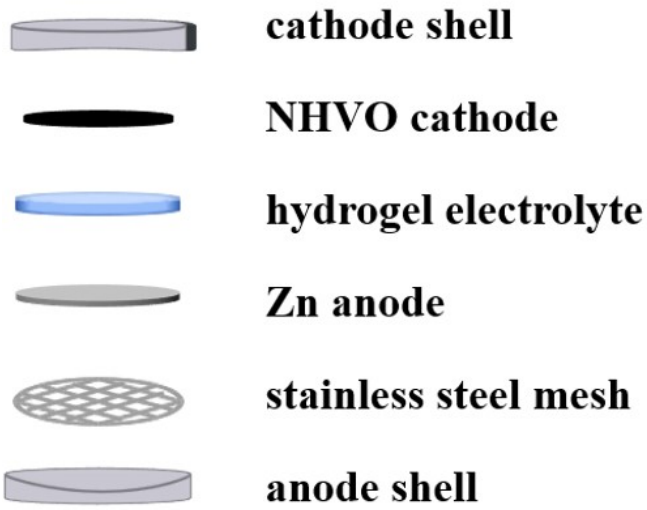

Figure S7. Zn||electrolyte||NHVO coin cell assembly flowchart

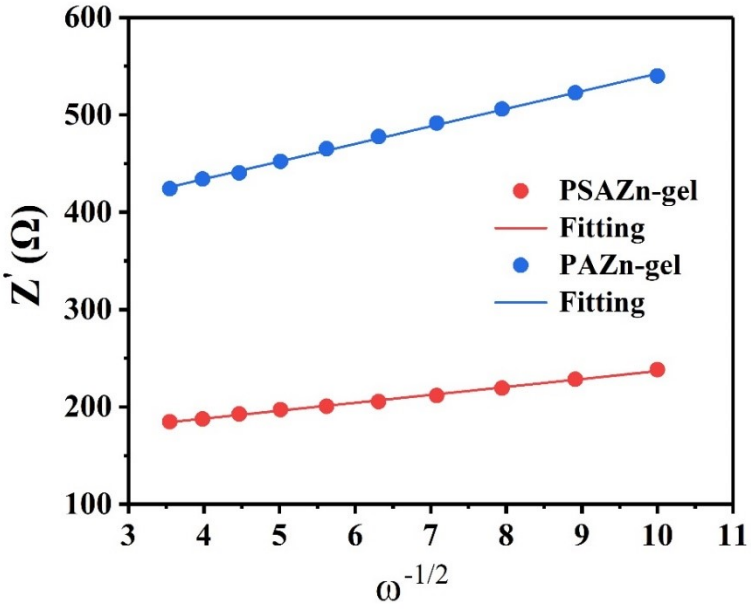

Figure S8. Linear fitting of the relationship between Z' and $\omega^{-1/2}$ in the low-frequency region in the EIS curves of PSAZn-gel and PAZn-gel

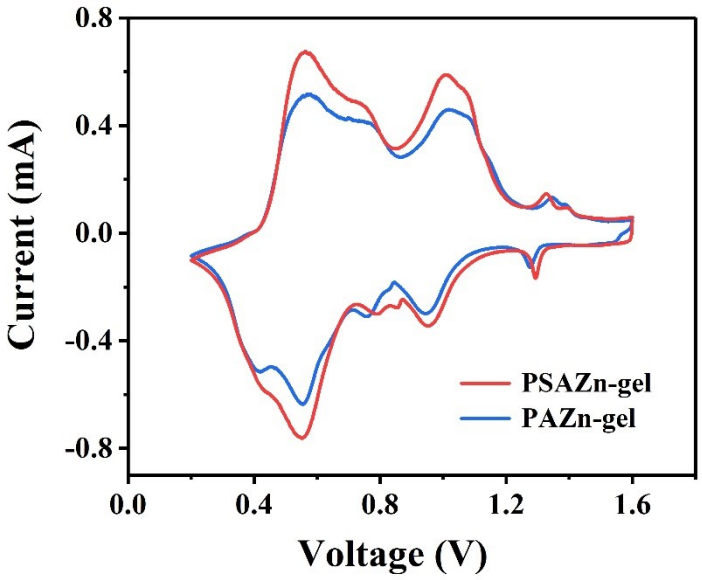

Figure S9. Second loop CV cycling curves of PSAZn-gel and PAZn-gel electrolytes at a scan rate of 0.2 mV s^{-1}.

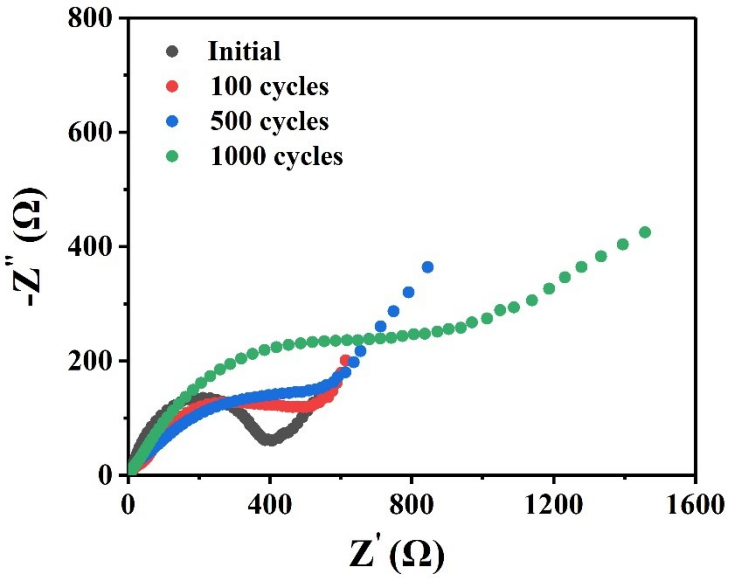

Figure S10. EIS changes of PAZn-gel electrolyte before and after cycling.

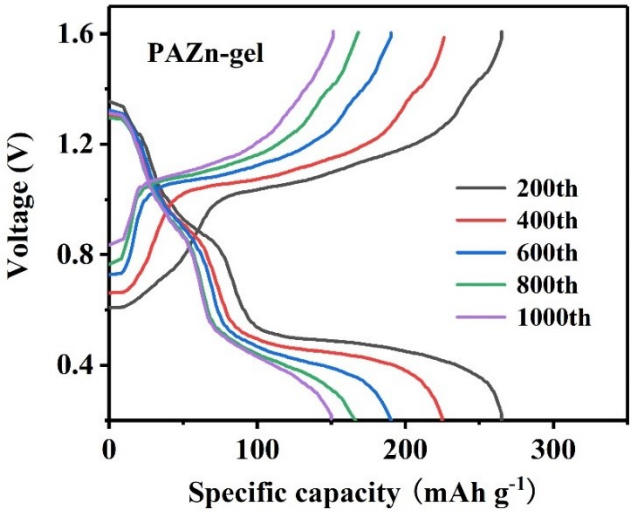

Figure S11. Charge/discharge curves at different cycle numbers of NHVO||PAZn-gel||Zn battery at 5A g^{-1}.

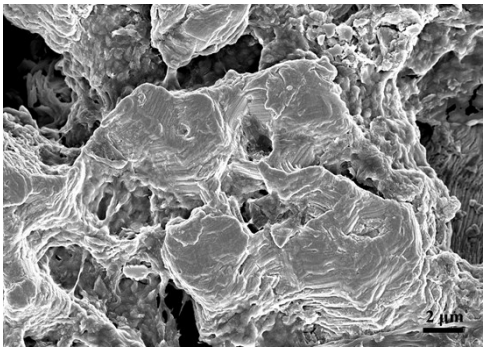

Figure S12. SEM images of Zn anode surface after 1000 cycles of NHVO||PSAZn-gel||Zn battery at 5 A g^{-1}.

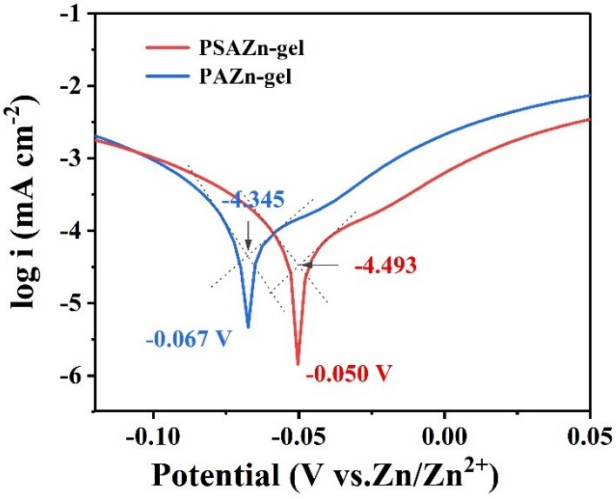

Figure S13. Tafel curves of the Zn anode in PSAZn-gel and PAZn-gel electrolyte.

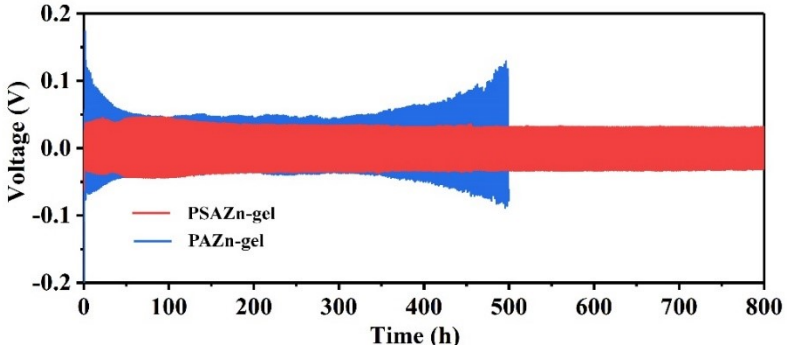

Figure S14. Cycling performance of the Zn symmetric cells at 1 mA cm^{-2} and 1 mAh cm^{-2}

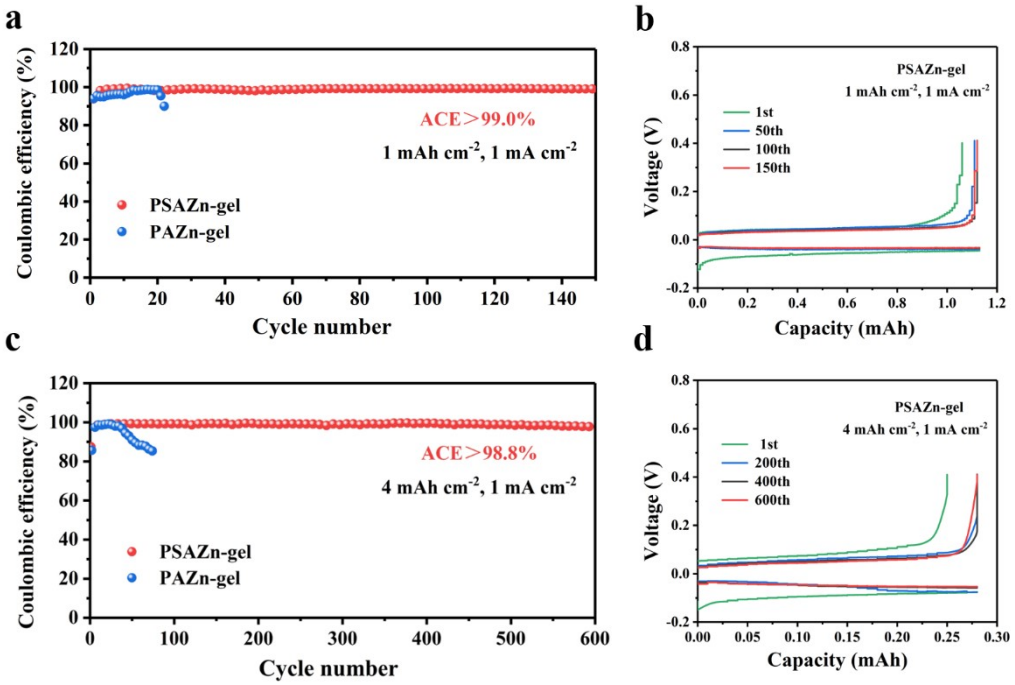

Figure S15. (a) Coulombic efficiency of Zn||Cu cells with PSAZn-gel and PAZn-gel electrolytes at 1 mA cm^{-2} and 1 mAh cm^{-2}. (b) Voltage-capacity curves of Zn||PSAZn-gel||Cu cell. (c) Coulombic efficiency of Zn||Cu cells with PSAZn-gel and PAZn-gel electrolytes at 1 mA cm^{-2} and 4 mAh cm^{-2}. (d) Voltage-capacity curves of Zn||PSAZn-gel||Cu cell.

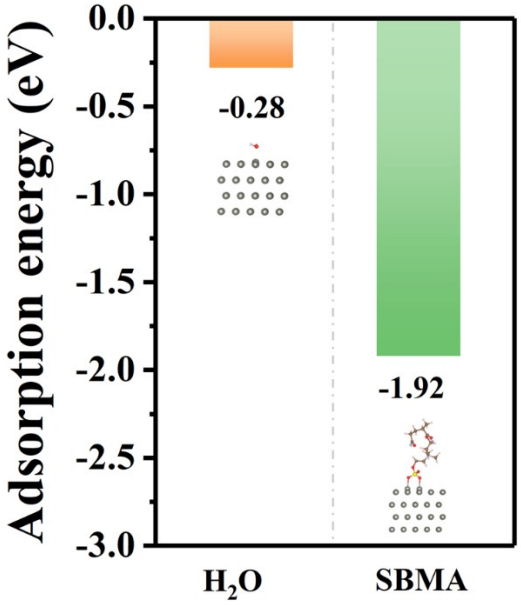

Figure S16. Adsorption energy calculations for Zn-H_2O and Zn-SBMA.

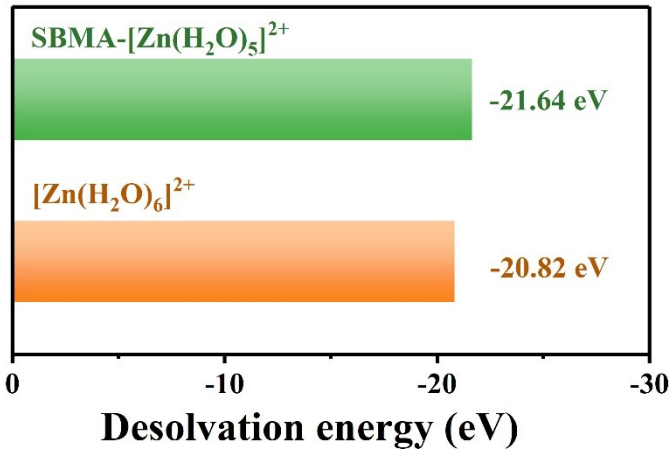

Figure S17. Desolvation energy calculations for SBMA-$[Zn(H_2O)_5]^{2+}$ and $[Zn(H_2O)_6]^{2+}$

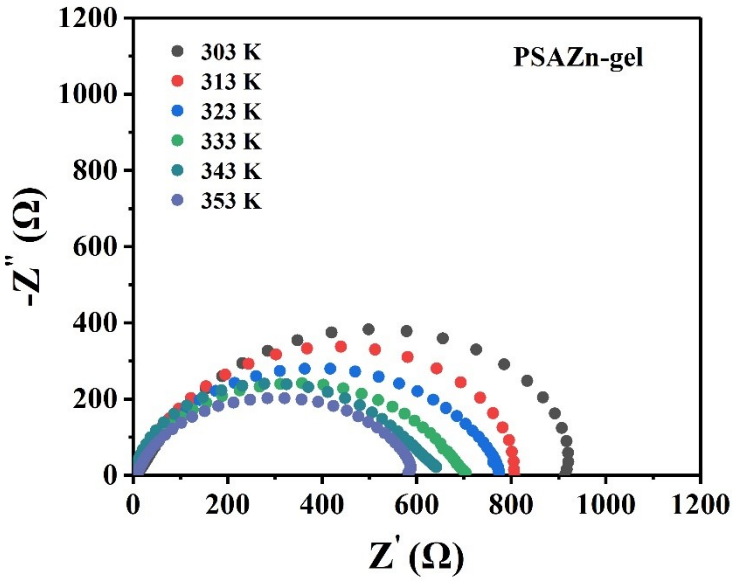

Figure S18. Nyquist plots of Zn||PSAZn-gel||Zn at different temperatures

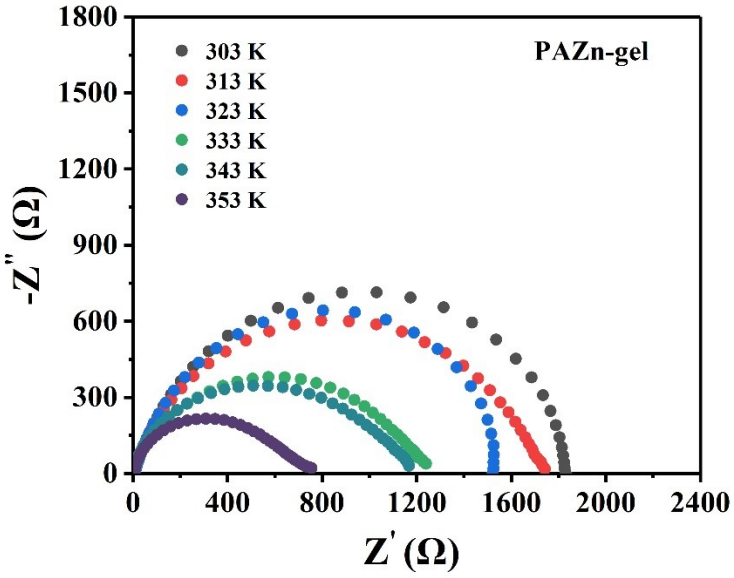

Figure S19. Nyquist plots of Zn||PAZn-gel||Zn at different temperatures

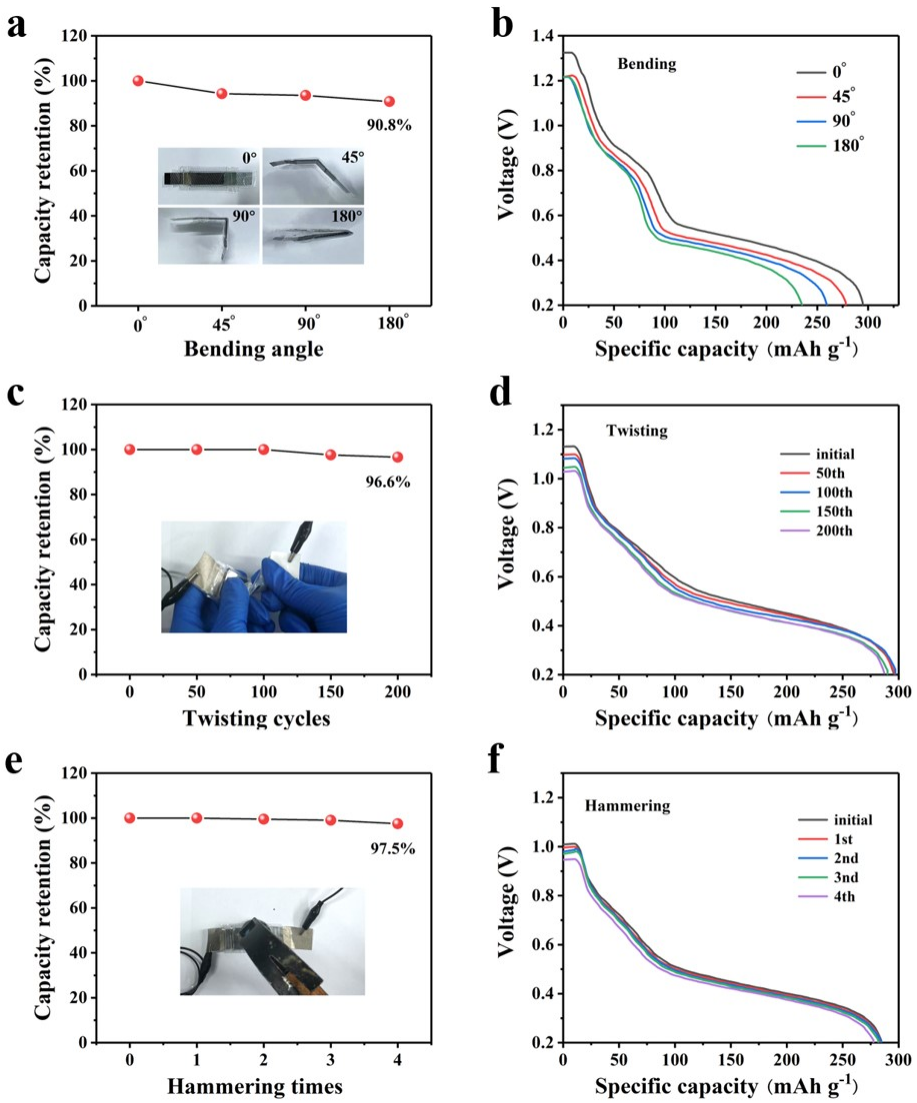

Figure S20. Electrochemical performance of flexible Zn||PSAZn-gel||NHVO batteries in different extreme tests. (a) Capacity retention and (b) charge/discharge curves of the bending test. (c) Capacity retention and (d) charge/discharge curves of the twisting test. (e) Capacity retention and (f) charge/discharge curves of the hammering test.

Table S1. Comparison of the performance of hydrogel electrolytes of different systems

Eletrolyte	Elongation	Substrate/Adhesion strength	Ionic conductivity (mS cm^{-1})	Zn^{2+} transference number	Ref.
This work	620%	Zn/108 kPa	59.0	0.81	
PAM/chitosan	> 150%	-	38.1	-	[1]
XG/PAM/CNF	-	Al/42.7 kPa	28.8	-	[2]
SA/AM/SBMA	310.20%	Zn/2.1-2.6 kPa	25	0.64	[3]
Con-CMC hydrogel	185%	-	34.5	-	
PAM/Al-Hbimcp	-	Zn/19.1 kPa	38.2	0.773	[4]
LCNFs/PAM	-	-	21.57	0.79	[5]
PAM/CMC/XG	443.70%	-	30	0.63	[6]
DMAPS/AAm/fiberglass	-	-	24.32	-	[7]
CMCS/PAM	> 600%	-	23.61	0.76	[8]
Carrageenan/wool keratin	≈720%	-	1.7	0.6	[9]
PVA/SA/XG/GA		-	18.86	0.8	[10]
AS/SAS-1.5	< 350%	-	29.2	0.616	[11]
CMC	185%	-	34.5	-	[12]
DAA/PAM	-	Zn/19.8 kPa	24.11	0.79	[13]
PAM/ xanthan gum	580%	Zn foil/3 kPa	16.8	-	[14]
TA/CNC/SBMA/AA	507%	Zn/ < 30 kPa	74.3	-	[15]

Reference

[1] Y. Q. Hu, Z. Wang, Y. Z. Li, P. W. Liu, X. L. Liu, G. X. Liang, D. Zhang, X. Fan, Z. G. Lu, W. X. Wang, Chemical Engineering Journal 2024, 479.

[2] B. J. Wang, J. M. Li, C. Y. Hou, Q. H. Zhang, Y. G. Li, H. Z. Wang, Acs Applied Materials & Interfaces 2020, 12, 46005-46014.

[3] T. L. Wu, C. C. Ji, H. Y. Mi, F. J. Guo, G. Z. Guo, B. Zhang, M. Z. Wu, Journal of Materials Chemistry A 2022, 10, 25701-25713.

[4] Z. J. Chen, T. Y. Shen, M. H. Zhang, X. Xiao, H. Q. Wang, Q. R. Lu, Y. L. Luo, Z. Jin, C. H. Li, Advanced Functional Materials 2024.

[5] Z. L. Li, G. Q. Zhou, L. Ye, J. Y. He, W. W. Xu, S. Hong, W. M. Chen, M. C. Li, C. Z. Liu, C. T. Mei, Chemical Engineering Journal 2023, 472.

[6] C. J. Jin, C. C. Yang, H. Y. Mi, C. C. Ji, F. J. Guo, C. Z. Liu, Z. Q. Liu, N. J. Yang, Journal of Energy Chemistry 2023, 86, 373-381.

[7] O. Zhanadilov, H. J. Kim, H. J. Lai, J. C. Jiang, A. Konarov, A. Mentbayeva, Z. Bakenov, K. S. Sohn, P. Kaghazchi, S. T. Myung, Small 2023, 19.

[8] S. W. Huang, L. Hou, T. Y. Li, Y. C. Jiao, P. Y. Wu, Advanced Materials 2022, 34.

[9] Y. Y. Shao, J. Zhao, W. G. Hu, Z. Xia, J. R. Luo, Y. J. Zhou, L. Zhang, X. Z. Yang, N. Ma, D. Z. Yang, Q. W. Shi, J. Y. Sun, L. Zhang, J. S. Hui, Y. L. Shao, Small 2022, 18.

[10] C. Y. Fu, Y. P. Wang, C. G. Lu, S. Zhou, Q. He, Y. Z. Hu, M. Y. Feng, Y. L. Wan, J. D. Lin, Y. F. Zhang, A. Q. Pan, Energy Storage Materials 2022, 51, 588-598.

[11] J. X. Li, J. F. Ren, C. X. Li, P. X. Li, T. T. Wu, S. W. Liu, L. Wang, Nano Research 2022, 15, 7190-7198.

[12] Y. H. Quan, H. Ma, M. F. Chen, W. J. Zhou, Q. H. Tian, X. Han, J. Z. Chen, Acs Applied Materials & Interfaces 2023, 15, 44974-44983.

[13] H. R. Wang, W. Wei, X. X. Liu, S. C. Xu, Y. F. Dong, R. H. He, Energy Storage Materials 2023, 55, 597-605.

[14] Y. Q. Deng, Y. H. Wu, L. L. Wang, K. F. Zhang, Y. Wang, L. F. Yan, Journal

of Colloid and Interface Science 2023, 633, 142-154.

[15] Q. J. Fu, S. W. Hao, L. Meng, F. Xu, J. Yang, Acs Nano 2021, 15, 18469-18482.